Molecular Dynamics Simulation of the Evolution of Hydrophobic Defects in One Monolayer of a Phosphatidylcholine Bilayer: Relevance for Membrane Fusion Mechanisms

D. Peter Tieleman* and Joe Bentz†

*Department of Biological Sciences, University of Calgary, Calgary, Alberta T2N 1N4, Canada; and †Department of Bioscience and Biotechnology, Drexel University, Philadelphia, Pennsylvania 19104 USA

ABSTRACT The spontaneous formation of the phospholipid bilayer underlies the permeability barrier function of the biological membrane. Tears or defects that expose water to the acyl chains are spontaneously healed by lipid lateral diffusion. However, mechanical barriers, e.g., protein aggregates held in place, could sustain hydrophobic defects. Such defects have been postulated to occur in processes such as membrane fusion. This gives rise to a new question in bilayer structure: What do the lipids do in the absence of lipid lateral diffusion to minimize the free energy of a hydrophobic defect? As a first step to understand this rather fundamental question about bilayer structure, we performed molecular dynamic simulations of up to 10 ns of a planar bilayer from which lipids have been deleted randomly from one monolayer. In one set of simulations, approximately one-half of the lipids in the defect monolayer were restrained to form a mechanical barrier. In the second set, lipids were free to diffuse around. The question was simply whether the defects caused by removing a lipid would aggregate together, forming a large hydrophobic cavity, or whether the membrane would adjust in another way. When there are no mechanical barriers, the lipids in the defect monolayer simply spread out and thin with little effect on the other intact monolayer. In the presence of a mechanical barrier, the behavior of the lipids depends on the size of the defect. When 3 of 64 lipids are removed, the remaining lipids adjust the lower one-half of their chains, but the headgroup structure changes little and the intact monolayer is unaffected. When 6 to 12 lipids are removed, the defect monolayer thins, lipid disorder increases, and lipids from the intact monolayer move toward the defect monolayer. Whereas this is a highly simplified model of a fusion site, this engagement of the intact monolayer into the fusion defect is strikingly consistent with recent results for influenza hemagglutinin mediated fusion.

INTRODUCTION

The hydrophobic effect is central to the formation of biological membranes, both lipid bilayer formation and membrane protein folding. The simplest description of the lipid bilayer is that all of the molecules are arranged to minimize the contact of their nonpolar atoms with water. However, the linear arrays of lipids shown in texts, aligned head to head and tail to tail, ignores the dynamic fluctuations that are being elucidated by molecular dynamics simulations (Tieleman et al., 1997; Feller, 2000; Lindahl and Edholm, 2001; Moore et al., 2001). One situation where these fluctuations must be important is during membrane fusion.

It is believed that the initial bilayer destabilization leading to fusion is initiated either through a high curvature bending defect (Chernomordik et al., 1998; Kozlov and Chernomordik, 1998; Siegel, 1999; Melikyan et al., 1999; Lentz and Lee, 2000) or a hydrophobic defect (Bentz, 2000a,b; Bentz and Mittal, 2000). These proposals agree on most points, including the appearance of lipid stalks (Chernomordik, 1996; Kozlov and Chernomordik, 1998; Kuzmin et al., 2001; Kozlovsky and Kozlov, 2002; Markin and Albanesi, 2002) to finally connect the outer monolayers. The question is how do the stalks form in the first place? What is the transition state for the formation of the stalk? It is generally believed that fusion proteins undergo an essential conformational change to create the initial defect for fusion (Skehel and Wiley, 1998; Eckert and Kim, 2001). The recipient of the energy released by this conformational change is the transition state of interest.

For the fusion mediated by influenza hemagglutinin (HA), an aggregate of eight or more HAs forms of which only two undergo a slow essential conformational change, which allows the first fusion pore to form (Bentz, 2000a; Mittal and Bentz, 2001; Mittal et al., 2002b). Kozlov and Chernomordik (1998) proposed a model for HA aggregation, wherein the fusion peptides are embedded in the viral envelope and the nascent conformational change to the extended coiled coil induces a curvature in the viral bilayer. An aggregate of HAs can stabilize this curvature in the form of a lipid dome with a "crown" of HAs. Kozlov and Chernomordik (1998) proposed that this dome interacts directly with the target membrane, and outer monolayer destabilization relieves the curvature stress at the tip of the dome. However, Bentz (2000b) argued that the fact that only two of the eight or more HAs in the fusogenic aggregate undergo the essential conformational change seems more consistent with a hydrophobic defect than a curvature defect. Within the HA aggregate proposed by Kozlov and Cherno-

Submitted January 29, 2002, and accepted for publication April 15, 2002.

Address reprint requests to D. Peter Tieleman, Department of Biological Sciences, University of Calgary, Calgary, Alberta T2N 1N4, Canada. Tel.: 403-220-2966; Fax: 403-289-9311; E-mail: tieleman@ucalgary.ca or to Joe Bentz, Department of Bioscience and Biotechnology, Drexel University, Philadelphia, PA 19104. Tel.: 215-895-1513; Fax: 215-895-1273; E-mail: bentzj@drexel.edu.

0006-3495/02/09/1501/10 $2.00

TABLE 1 Overview of the simulations

Name	Length	Description
REF	8 ns	Simulation of a bilayer of 2 × 64 lipids with constant area. No lipids have been removed, and no lipids are subject to position restraints.
R0	6 ns	Simulation of a bilayer of 2 × 64 lipids with constant area in which 29 lipids in one leaflet of the bilayer have been harmonically restrained to stay near their initial position.
R3	6 ns	Simulation of a bilayer with constant area, consisting of 64 lipids in one leaflet and 61 lipids in the other, "defect" leaflet. The same 29 lipids as in R0, in the defect leaflet, have been harmonically restrained to their initial position.
R6	10 ns	The same as R3 but with 58 lipids in the defect leaflet instead of 61.
R9	10 ns	The same as R6 but with 55 lipids in the defect leaflet instead of 58.
R12	10 ns	The same as R9 but with 52 lipids in the defect leaflet instead of 55.
R12F	4 ns	Simulation of a bilayer with constant area, consisting of 64 lipids in one leaflet and 52 in the other, "defect" leaflet. All lipids are free to move, without harmonic restraints.
R18F	4 ns	The same as R12F, but with 46 lipids in the defect leaflet instead of 52.

mordik (1998), the conformational change of two HAs to the extended coiled coil would leave a hydrophobic cavity in the center of the HA aggregate, stabilized by the "dam" of transmembrane domains, and remaining fusion peptides (see also Bentz and Mittal, 2000).

How this curved bilayer can initiate the fusion is unknown and quite difficult to probe experimentally. This suggests the value of a molecular simulation to assess the structure of the site. The proposed fusion site with both the proteins and the curved bilayer is too complex to simulate at present. However, we can investigate the simplest element, i.e., what would happen if a persistent hydrophobic defect were formed in a bilayer? How would the hydrophobic effect heal this wound without the help of lipid lateral diffusion according to a molecular dynamics simulation? We used a planar bilayer patch of 8 × 8 equilibrated phosphatidylcholine (PC) molecules in water and deleted 0, 3, 6, 9, or 12 of the PCs from one monolayer while restraining part of the lipids to act like a wall such as might be formed by transmembrane domains and the remaining embedded fusion peptides of the HAs, as described above. This created several persistent hydrophobic defects in the patch, because there are no extra lipids to diffuse into the patch. Our question was simply whether the hydrophobic defects in the patch would percolate together, making a single large hydrophobic cavity, or whether they would increase their acyl chain cross-sectional area and "squat down" to achieve acyl chain contact throughout the defect monolayer. For comparison, we also studied two bilayers in which lipids were removed from one monolayer but no further restraints were applied. Our results suggest that simulations on curved bilayers with persistent hydrophobic defects, when feasible, will predict an even more realistic fusion site.

MATERIALS AND METHODS

Simulations were carried out with Gromacs (Berendsen et al., 1995; van der Spoel et al., 1999). The united atom lipid parameters are based on Berger's parameters (Berger et al., 1997) with additional parameters for the unsaturated carbons taken from GROMOS87. Water was modeled as simple point charge (Berendsen et al., 1981). All simulations used a twin-range cutoff for Coulomb of 1.0/1.8 nm and a single cutoff for Lenard-Jones interactions of 1.0 nm. Temperature and pressure were controlled using the weak coupling algorithm (Berendsen et al., 1984) with $\tau_T = 0.1$ ps, $T = 300$ K, $\tau_p = 1.0$ ps, with a pressure of 1 bar in the z direction. The timestep used was 2 fs with a neighbor list update every 10 steps. Coordinates were saved every picosecond. A structure from a previous simulation was used as starting structure for the 128 lipids palmitoyl-oleoyl-phosphatidylcholine bilayer (available from http://moose.bio.ucalgary.ca) (Tieleman et al., 1999). Extra water was added, for a total of 4480 water molecules and 128 lipids (20,096 atoms), resulting in a system of 6.37 nm × 6.59 nm × 7.14 nm. A short equilibration run of 25 ps was used to equilibrate the added water. The lateral area was kept fixed in all simulations described, at an area of 0.655 nm^2 per lipid, whereas the z dimension of the box was allowed to fluctuate. The area was estimated based on the experimental area of DPPC of 0.629 ± 0.014 nm^2 (Nagle et al., 1996). However, the area is not critical in the current set of simulations. An overview of the simulations is given in Table 1. For simulations R0 to R12, 29 lipids that approximately form the edge of one of the two bilayer monolayers were restrained with an harmonic position restraint on all atoms of 1000 kJ mol^{-1} nm^{-1}. From the remaining 64 − 29 = 35 lipids that were free to move in this monolayer, between 0 (R0) and 12 lipids (R12) were removed randomly to create a hydrophobic defect (Fig. 1). The resulting structures were used as starting structures for simulations R0 to R12. Water atoms rapidly (within 50 ps) fill the vacuum created by removing lipids as the pressure coupling in the z direction automatically reduces the total volume of the system according to the number of lipids that has been removed. Lipids also readjust somewhat during this fast initial equilibration, but their motions are much slower than the diffusion of water. For R12F and R18F, 12 or 18 lipids were removed from one monolayer, but no lipids were fixed at their positions. Analyses were done with Gromacs programs (Berendsen et al., 1995; van der Spoel et al., 1999). Molecular graphics were made with molscript (Kraulis, 1991) and raster3D (Merritt and Bacon, 1997).

RESULTS

Our primary goal is to determine how lipids adjust to a hydrophobic defect in one monolayer. To do this, we monitored the solvent accessible area of groups of lipids, the depth in the bilayer of several atoms along the lipid chains, and the average distance from the phosphorus atom to the last carbon of the palmitoyl chain during the simulations. We also calculated the deuterium order parameters for the chains and the atomic density profiles across the membrane over the last part of each simulation. Combined with mo-

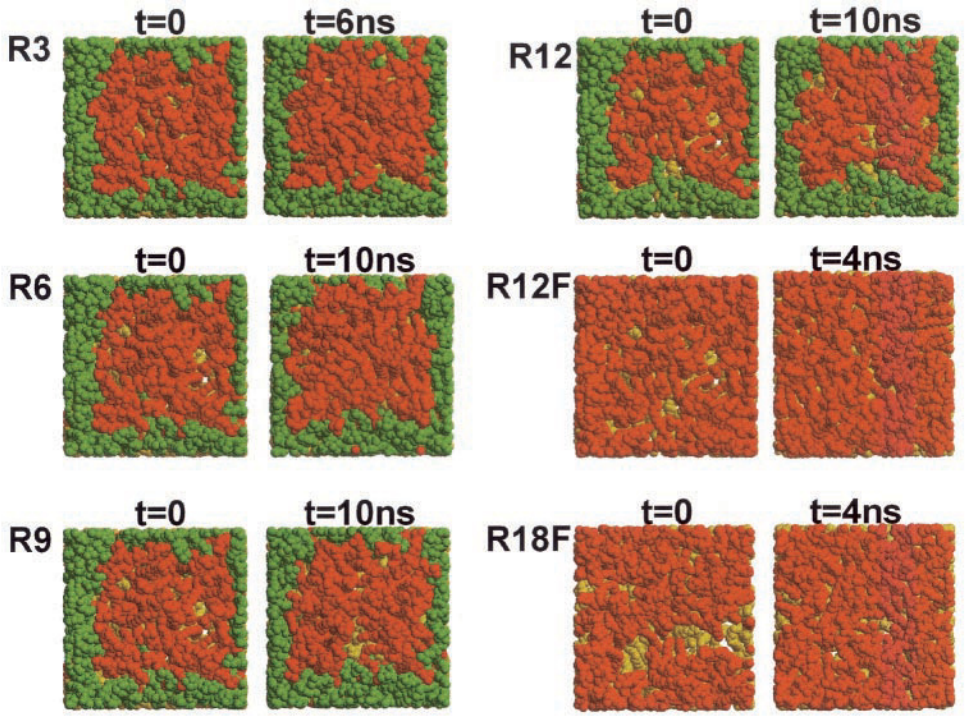

FIGURE 1 Selected molecular graphics views of the simulations, showing the effect after equilibration of introducing defects of various degrees of severity. Shown are views of R3, R6, R12, R12F, and R18F; R0 and REF differ only marginally from R3 in these views. In all images, position-restrained lipids are green, freely-moving lipids in the defect monolayer are red, and lipids in the opposing monolayer are yellow. All oxygens are red, phosphorous pink, and nitrogen blue. In all cases, the initial structure looking down on the defect monolayer is shown, together with the final structure after the indicated time.

lecular graphics pictures of the starting and the final structures of each simulation these properties allow a reasonable description of the evolution of a hydrophobic defect.

Molecular graphics

Fig. 1 shows molecular graphics views of the lipid bilayer with different defects. R0 to R12 all have 29 lipids restrained in one monolayer of the bilayer (green). Of the remaining 35 lipids, 0 to 12 lipids are randomly removed (red). These lipids will be referred to as "free lipids." The monolayer with the defect will be referred to as the "defect monolayer." The other monolayer is colored yellow, which will be referred to as the "intact monolayer." The z axis runs perpendicular to the lipid-water interface across the bilayer. It should be noted that the snapshots give an impression of the different states and different views of the bilayer, but that significant fluctuations occur. Nonetheless, the general results of the simulations are already visible. In R0 and REF (both not shown), the red and green lipids cover the view from above entirely, and no yellow lipids are visible. In R3, the free lipids redistribute and cover as much of the holes as possible. In R6 this is still reasonably effective. In R9 and R12, the free lipids are unable to cover the yellow lipids effectively. In R12F and R18F, the lipids in the defect monolayer spread out and thin significantly. This general picture is confirmed by the more detailed analyses below. These analyses will also describe what happens to the intact bilayer, which is harder to visualize.

Average lipid length and position

It is useful to consider the positions of different atoms within the lipids as well as the overall length of the lipids to determine how the lipids adjust to the presence of a defect. We have chosen to monitor a few key atoms: P8, the phosphorus atom; C13, the middle carbon atom of the glycerol group; C24, the 9th carbon of the oleoyl chain; C42, the 8th carbon of the palmitoyl chain, and C50, the last carbon (CH_3) of the palmitoyl chain, all counting from the headgroup to the end of the tails. Fig. 2 shows the average z coordinate of each of these groups of atoms for the free lipids in the defect monolayer and all the lipids in the intact monolayer. The results for R12F and R18F are relatively straightforward: atoms along the whole lipid are hardly affected in the intact monolayer, but in the defect monolayer all move closer toward the center. Not surprisingly, the effect is largest for atoms furthest away from the center. This is consistent with the molecular graphics in Fig. 1. The z position of atoms in R0 to R12 is more interesting. Not much change is observed in R0 (or in REF, data not shown) and little change in R3. However, R6 to R9 P8 and C13 in the defect monolayer move somewhat closer to the center. C24, C42, and C50 show less change except in R12, where all three clearly move toward the center. Interestingly, the average position of atoms in the intact monolayer also moves closer to the center. Lipids from the intact monolayer move in from the other side to fill in some of the gaps. However, the average z positions of C50 in both monolay-

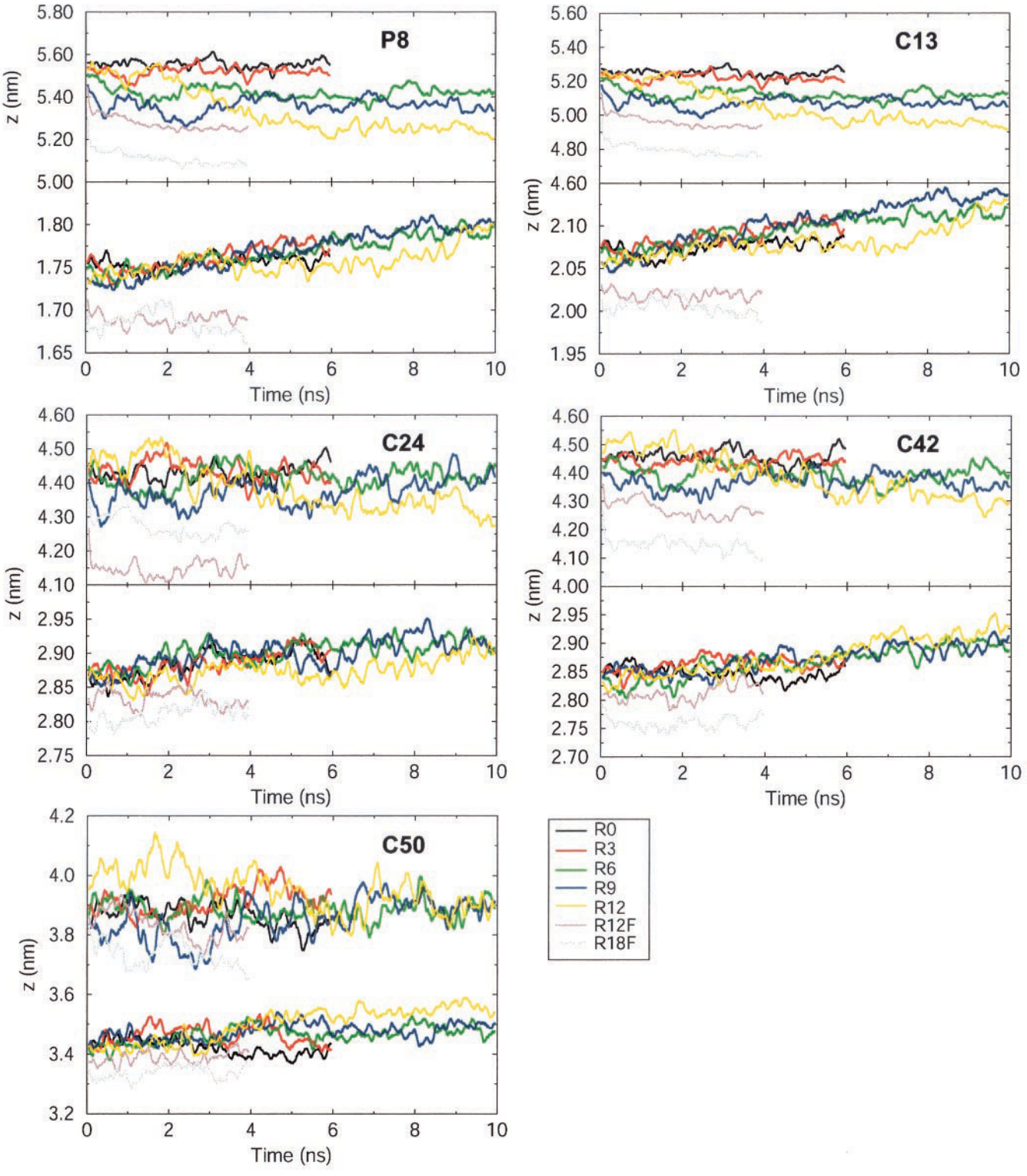

FIGURE 2 Average z coordinate of selected atoms as function of time for the different simulations. These graphs indicate how much (parts of) the lipids move laterally in reaction to the formation of a defect. In particular, for larger defects the lipids in the intact leaflet move significantly toward the defect leaflet. For the defect monolayer, only free lipids are taken into account. For the intact monolayer we averaged over all lipids. P8 is the phosphorous atom, C13 is the middle carbon atom of the glycerol group, C24 is the 9th carbon of the oleoyl chain, C42 the 8th carbon of the palmitoyl chain, and C50 the last carbon (CH_3) of the palmitoyl chain, all counting from the headgroup to the end of the tails.

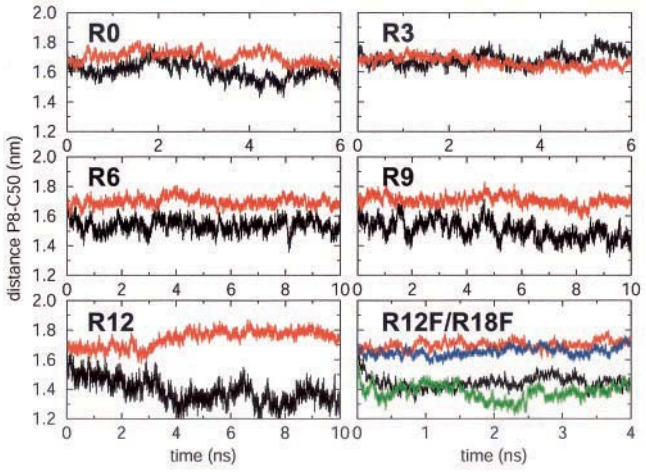

FIGURE 3 Average distance from the phosphorus atom (P8) to the last carbon atom of the palmitoyl chain (C50) for the free lipids in the defect (*black*) and the intact monolayer (*red*). These distances can be interpreted as the length of a lipid, which depends on the size and type of defect present. For R18F the intact monolayer is blue, the defect monolayer green.

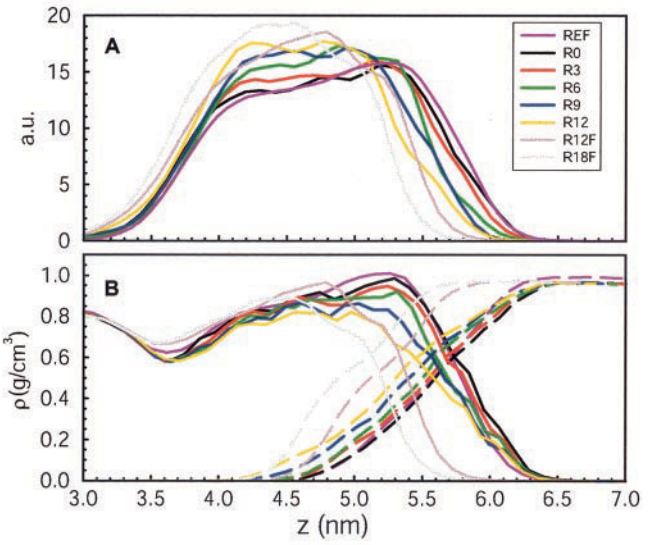

FIGURE 4 Density profiles indicating the distribution of free lipids in the defect monolayers and the water penetration into the defect monolayer. (*A*) Total lipid density and the total water density for the defect side of the bilayer is shown for each of the simulations. (*B*) Distribution of just the free lipids in the defect area is given. The distribution has been normalized to the number of lipids that are free to move around and is in arbitrary units on the *y* axis. The distribution of lipids shows a systematic shift of the free lipids in the defect leaflet toward the center as more and more lipids are removed.

ers, the last atom of the palmitoyl chain, still differs by 0.4 nm, showing that there is no average interdigitation of the lipids. In an equilibrium bilayer, without defect, the terminal methyl groups of both chains are distributed over the same range of z coordinates, and the distributions for both monolayers overlap. Although the terminal methyl distribution in R12 overlaps more than in an unperturbed bilayer, interdigitation of more than these methyl groups remains small. An interesting question is how the structure of the lipids is changing. A simple criterion to monitor is the "length" of a lipid, taken as the average distance between P8 and C50 in a lipid. Fig. 3 summarizes the lipid length as a function of time. The black lines, the free lipids in the defect monolayer, show that going from R0 to R12 the lipid length decreases substantially from ~1.6 nm to ~1.3 nm for R12. The red lines, the intact monolayers, show that the lipid length in the intact monolayers is mostly unaffected. An exception is R12, where it appears that the lipid length of the free lipids increases somewhat. This correlates with the increase in order parameters for this system (see below). Thus, although the lipids in the intact monolayers show an increasing tendency to move toward the center when removing more and more lipids in a defect in the other monolayer, this has little effect on the average length of the lipids. In R12F/R18F, the lipid length in the intact monolayer increases (blue line for R18F), but the lipid length of the lipids in the defect monolayer rapidly decreases (~0.5 ns) from 1.6 to 1.7 nm to 1.4 to 1.3 nm.

Density profiles

In Fig. 4 *A* the normalized distribution of the free lipids in the defect monolayer is plotted. REF (averaged over all 64 lipids in one monolayer, because there are no restrained lipids) and R0 are similar with small differences due to the restraints in R0. From R0 to R3 to R6 to R9 to R12, the distribution becomes increasingly sharper and shifts to the middle of the bilayer, consistent with the analyses already presented. The effect is even stronger for R12F and R18F (both averaged over all lipids in the defect monolayer), both of which narrow and shift toward the middle of the membrane. In the same order, water penetration increases from R0 to R18F, as shown in Fig. 4 *B*. Note that in Fig. 4 *A* the lipid distribution is normalized on the number of lipids, whereas the values in Fig. 4 *B* are absolute in g/cm^3. The minimum in the total lipid density profile changes little between the different simulations.

Order parameters

A more detailed method to study the change in conformation of lipids is to consider "deuterium" order parameters, calculated from the simulations. In Fig. 5, these are shown for R0 to R12 and R12F/R18F, split in four groups: free lipids in the defect region for the first part of each simulation, free lipids in the defect region for the last part of each simulation, and the same for the lipids in the intact monolayer. This allows an approximate view of the time evolution of the order parameters or the adjustment of the lipids after the sudden creation of a hydrophobic defect. Note that

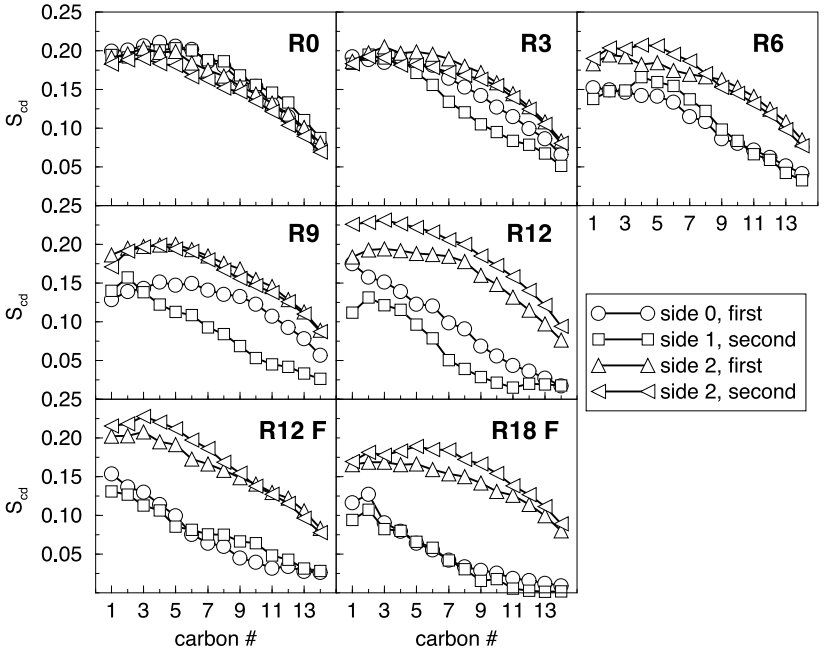

FIGURE 5 Deuterium order parameter profiles for the palmitoyl chains. Side 1 refers to the defect monolayer, and Side 2 refers to the intact monolayer. First and second indicate two parts of the simulation that were used to calculate the order parameters shown: for R0 and R3, 0 to 3 ns and 3 to 6 ns; for R6 to R12, 0 to 3 ns and 7 to 10 ns; and for R12F and R18F, 0 to 2 ns and 2 to 4 ns. Data for simulation REF are not shown, as they are indistinguishable from R0.

the order parameters are shown for carbons 2 to 15 of the palmitoyl chain of the lipid. Again, let us consider R12F/R18F first. In both of these cases, there is a fast and very large drop in order parameters for the lipids in the defect monolayer, consistent with the observed thinning. The drop is fast because there is little difference between the order parameters averaged over 0 to 2 ns and 2 to 4 ns in both cases.

The intact monolayer is affected somewhat with a small increase in order along most of the chain. The last seven carbons in R18F have essentially random order. In R0, there is little difference between the four graphs, as expected. In R3, however, it is clear that a significant drop in order parameters develops in the course of the simulation for the free lipids in the defect area over the last 10 carbons of the tail. This suggests that the bilayer structure near the upper ends of the chains does not change much but that the "floppy" ends of the chains readjust to attempt to fill the extra free volume.

The effects on R6, R9, and R12 become progressively stronger with the presence of larger defects. The order parameters for the free lipids in the defect area continue to drop, along the whole chain including the atoms close to the lipid glycerol moiety. However, in R6 and R9 there is still little effect on the chain order of the lipids in the intact monolayer. In R12, there is some increase along the whole chain for the lipids in the intact monolayer, consistent with the increase in lipid length discussed above. Comparison of order parameter profiles between R12F and R6 and R18F and R9 shows that the presence of restrained lipids significantly limits the effect of removing lipids. R12F has a relative surface concentration of $(64 - 12)/64 = 0.81$, comparable with R6 with $(35 - 6)/35 = 0.83$. R18F has a surface concentration of $(64 - 18)/64 = 0.72$, comparable with R9 with $(35 - 9)/35 = 0.74$. Thus, the changes in lipid structure cannot be explained by just a change in surface concentration.

Solvent accessible area

The driving force for the behavior of hydrophobic defects will be to a large extent the solvent-accessible hydrophobic area. Fig. 6 follows the hydrophilic (Fig. 6 *A*) and hydrophobic (Fig. 6 *B*) solvent accessible area per lipid for the free lipids in the defect area. These graphs also give an indication of the timescale of the readjustment of the lipids and the degree of equilibration in our simulations. Like the order parameters, the solvent accessible areas for R12F and R18F show a rapid decrease after the creation of the initial defect within a few hundred picoseconds. The relaxation times for the other systems increase with the size of the defect and are of the order of 5 ns. This is quite fast relative to the normal time scales of lipid motion in bilayers (Lindahl and Edholm, 2001), indicative of the large driving forces present in the system.

The areas appear to converge to a predictable order with the hydrophobic solvent accessible area increasing from R0 to R3 to R6 to R9 to R12. R12F and R18F have a remarkably low solvent accessible area, demonstrating that the presence of restraints on the lipid motions significantly changes the behavior of the remaining free lipids. In Fig. 7, the average solvent accessible areas are shown as a function of defect size, averaged over the last part of each simulation.

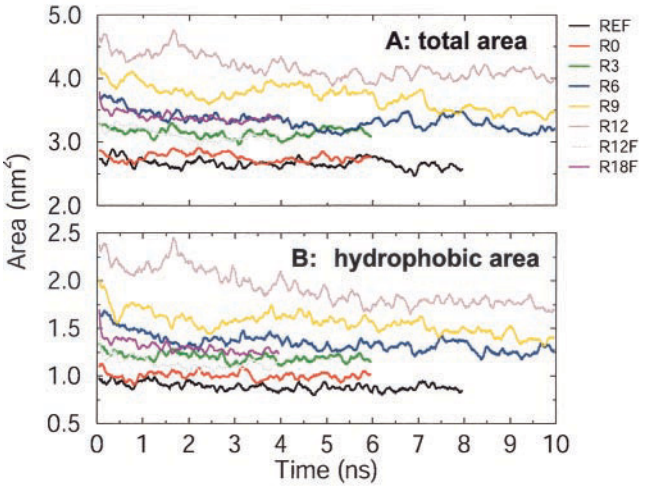

FIGURE 6 Solvent accessible surface area per lipid for the free lipids in the defect area. (*A*) Hydrophilic accessible surface area is shown. (*B*) Hydrophobic solvent accessible surface. An atom is defined as hydrophobic if its partial charge is less than 0.3 e, which is only true for the carbons of the tails, without the carboxyl carbon.

For both the hydrophilic (Fig. 7 *A*) and the hydrophobic (Fig. 7 *B*) solvent accessible area there is a steady increase for all three groups of lipids: Grp 1 consists of the restrained lipids, Grp 2 consists of the free lipids in the defect area, and Grp 3 consists of all lipids of the intact monolayer. The increase is most dramatic for the free lipids in the defect area and occurs for both hydrophobic and hydrophilic atoms. Fig. 7, *C* and *D* show that the solvent accessible area, both hydrophobic and hydrophilic, increases significantly for the defect monolayer of R12F and R18F compared with

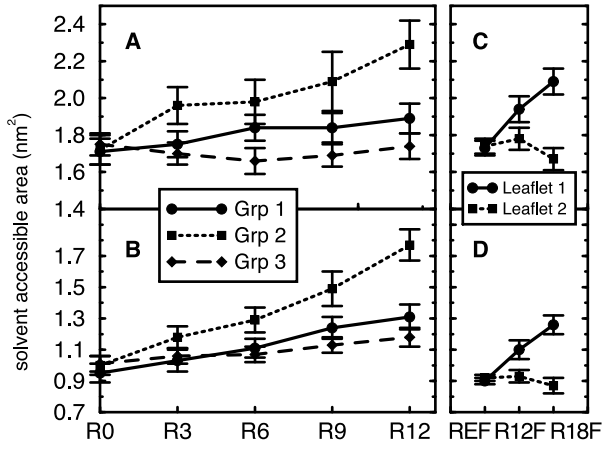

FIGURE 7 Total (*top*) and hydrophobic (*bottom*) solvent accessible areas, averaged over the last part of each simulation: 3 to 6 ns for REF, R0 and R3, 7 to 10 ns for R6 to R12, and 2 to 4 ns for R12F and R18F. Grp1 indicates lipids 1 to 29 that are restrained in the defect layer, Grp2 are the free lipids in the defect monolayer, and Grp3 are the lipids in the intact opposing monolayer. For REF, R12F, R18F Grp1 is the defect monolayer, Grp2 the intact opposing monolayer.

REF, without defect, but the intact monolayer is almost unaffected. This again demonstrates the effectiveness of the free lipids to cover all exposed chains from the intact monolayer by thinning substantially.

DISCUSSION

Hydrophobic defects in lipid bilayers

The simulations presented in this paper are used to investigate qualitatively how hydrophobic defects that arise in nonequilibrium processes might evolve. We considered two cases. In the most interesting case, the flow of lipids to a defect is restricted by mechanical barriers, here represented by position restraints on a subset of the lipids. For comparison, we also considered defects in a lipid monolayer where lipid flow is unrestricted. When there are no mechanical barriers, the adjustment of lipids to the presence of a defect appears straightforward. The lipids spread over the available surface, decreasing the monolayer thickness but with only a relatively small effect on the final hydrophobic solvent accessible area. The intact monolayer is hardly affected by this process.

When a mechanical barrier is present, the behavior of the remaining lipids in the defect area is more complex. The main effect of randomly removing lipids is still a thinning effect that becomes stronger with the size of the defect. In R3, with three lipids removed, the lower one-half of the chains becomes more disordered, but the headgroup region and the upper part of the chains remains more or less the same. There is little effect on lipid length and on the opposite monolayer. However, in R6, R9, and R12, an additional change occurs. The lipids in the defect area do not thin as much, and there is a coupling with the intact monolayer. The larger the defect, the more lipids from the intact monolayer move toward the defect. In the case of R12, this leads to "stretching" of the lipids from the intact monolayer with increased order parameters and an increased length.

In retrospect, and in an overly simplified way, this is what would be expected if the hydrocarbon cores were treated as a continuous fluid with an initial water filled cavity in the defect monolayer. The area of contact with water for the unconstrained system would be less with thinning than with retaining the cavity, since the surface area of polar headgroups would be the same in both cases. When the defect perimeter lipids were fixed in place, thinning of the defect monolayer is constrained by the exposure of the acyl chains of the fixed lipids. The acyl chains of the intact monolayer were drawn into the defect, because the defect monolayer could not thin as much as in the unconstrained case. If we push the continuous fluid analogy still further and assume we fix the hydrophobic perimeter through both monolayers, as a protein transmembrane domain would be, we would expect that the additional restraint on thinning of

the intact monolayer would constrain further the thinning of the defect monolayer. Perhaps, some degree of cavitation in the defect monolayer might occur. This remains to be investigated.

Simulation assumptions and limitations

It is useful to consider some choices made in the design of our simulations and some limitations. There are several possible approaches to considering defects within a restricted area. We chose to restrain a "ring" of lipids in the "outer" monolayer to provide a barrier to the defect zone, on the assumption this roughly resembles the situation where fusion proteins inhibit lipid flow. Alternative approaches could have included perfectly cylindrical walls modeled as some potential or actual proteins or protein models that form a restricted zone. Model potentials would have provided unknown interactions between the walls and the free lipids and would have required considerable investigations into the effect of different types of walls. Protein models would have considerably increased the complexity and the number of atoms of the systems studied. With the relatively long relaxation times on a 5- to 10-ns timescale, this would have made the computation too expensive at present.

One further design simplification that deserves some attention is our choice to restrain only lipids in one monolayer of the membrane, whereas fusion protein transmembrane domains span both monolayers. Lipids are so disordered that it would be problematic to identify a "ring" of lipids in the intact monolayer that have the same lateral location as in the defect monolayer to mimic a cylindrical restraint. In the end, we believe that the trends identified in our simulations are qualitatively accurate, as will be elaborated just below.

The simulations have several limitations. In particular, the length of the simulations with larger defects (9–12 lipids removed) appears only a few nanoseconds longer than the necessary minimal length to see the major adjustments of the system. It is possible that considerably longer relaxation times are present in some of the systems, although there are no clear indications for this. A second limitation is the use of electrostatic cutoffs, which are likely to affect the structure of the bilayers to some extent. However, due to the qualitative nature of these simulations we do not believe this is a major concern. For example, in a recent paper by Marrink et al. (2001), PC lipids reorganized from random orientations in water into a bilayer even when long range electrostatic interactions were not taken into account beyond 1.7 nm.

Implications for fusion

Whereas our direct goal here was to investigate the evolution of persistent hydrophobic defects in a monolayer, we want to return briefly to the molecular situation during membrane fusion, one case where we suggest they could arise. If the hydrophobic defect is a necessary step in influenza hemagglutinin mediated fusion, as proposed (Bentz, 2000b; Bentz and Mittal, 2000; Mittal and Bentz, 2001), then the very simplest version had the persistent hydrophobic defects coalesce together, to provide a clear target for lipids permeating from the defect monolayer of the target membrane. This, however, did not occur in the simulation, but what did occur suggests a more realistic scenario, which is consistent with the most recent and rigorous findings about HA-mediated fusion.

Two recent studies can shed much light on our results by focusing our attention on what might be expected at a successful fusion site. First, Mittal et al. (2001, 2002a) used automated video fluorescence microscopy to analyze lipid and contents mixing kinetics between individual red blood cell/erythrocyte-HA expressing cell pairs. For those pairs showing lipid mixing, one of two phenotypes was observed. There were those that completed fusion, where aqueous contents and both lipid monolayers mix, and those that showed only hemifusion, presumably a mixing of only the outer monolayers. Remarkably, starting from the onset of lipid mixing, fusion (with contents mixing) was completed more quickly than hemifusion, suggesting that these two phenotypes arise from (at least) two distinct defects.

In a second study, the protein basis for these two distinct defects was suggested. Leikina et al. (2001) found that a soluble proteolytic fragment formed from the low pH form of HA (FHA2, Kim et al., 1998) could induce only hemifusion between cells at low pH, i.e., mixing of outer monlayer lipids only. This fragment is essentially the low pH equilibrium structure for HA2, i.e., with preformed extended coiled coil and helix-turn. Generally, the soluble amphipathic peptides seem only able to destabilize the defect monolayers enough to provoke hemifusion (for review, see Bentz and Mittal, 2000), i.e., the inner monolayers are not coupled to the defect formed. Thus, for successful fusion, the fusion proteins must couple the viral inner monolayer into the defect.

In one sense it is obvious that fusion, by definition the complete mixing of lipids and aqueous contents, requires the participation of the intact monolayers (Bentz and Ellens, 1988). The question is: What is the molecular meaning of "coupling" the intact monolayer to the fusion defect? It is known that HA-mediated fusion requires the essential conformational changes of HA (Qiao et al., 1998) and a full transmembrane domain (Armstrong et al., 2000; Bentz, 2000b), i.e., HAs with truncated transmembrane domains provoke only hemifusion. So how do these factors engage the inner monolayer into the initial fusion defect?

Our simulation showed a coupling of the intact monolayer with the defect when the defect perimeter lipids were fixed and six or more lipids were removed. This break point is interesting because two bilayer-embedded HA fusion peptides would occupy about the same surface area as six or

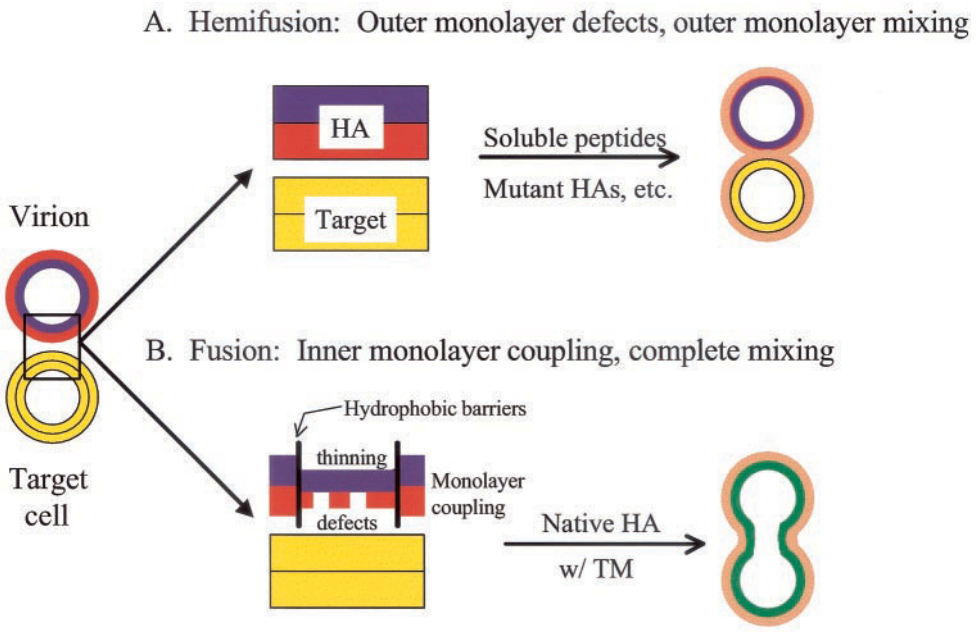

FIGURE 8 Schematic picture showing the requirements found for differentiating defects, which lead to hemifusion from those that lead to fusion with contents mixing and complete lipid mixing. Thus far, soluble peptides and defective HA aggregates only destabilize the outer monolyers, leading to hemifusion, as shown in *A*, where the red and yellow outer monolayers mix to form orange. Fusion, with contents mixing, requires coupling the inner monolayers to the fusion defect. Here we have found that persisent hydrophobic defects constrained within a hydrophobic barrier lead to the inner monolayer encroaching into the defect monolayer. This is the first instance of a viable fusogenic defect. Membrane curvature and transbilayer hydrophobic barriers, like protein transmembrane domains, are likely to result in more realistic fusion sites.

so lipids so that their removal would create about the same sized hydrophobic defect. So in the proposed fusogenic HA aggregate (Bentz, 2000b; Bentz and Mittal, 2000), the removal of two embedded fusion peptides from the center of the fusogenic aggregate would create a large enough hydrophobic defect to cause the intact monolayer acyl chains to enter into the defect area of the defect monolayer because of the hydrophobic transmembrane domains. Provided that the "dam" of HAs remains intact, this scenario is reasonable and provides a first guess as to the molecular definition of "coupling," which can distinguish between the defects that lead to fusion from those which lead only to hemifusion. That is, amphipathic peptides (Leikina et al., 2001; Bentz and Mittal, 2000), low surface densities of HA (Chernomordik et al., 1998), and some mutant HAs (Qiao et al., 1998, 1999; Armstrong et al., 2000; Melikyan et al., 1999) only disturb the outer monolayers leading to hemifusion. Here we have an example of how a hydrophobic defect in the lipid defect monolayer, if surrounded by a hydrophobic mechanical barrier, will engage the inner/intact monolayer. This is summarized in Fig. 8. Clearly, it is possible that there are other mechanisms to engage the intact monolayer. For example, rapid removal of the fusion peptide might have not only local effects on the defect leaflet but on the intact leaflet as well. This could be investigated by further simulations but is outside the scope of this study.

We are a long way from fusion and from the formation of a hydrophobic cavity. However, our simulation neglected two elements that seem likely to favor percolation of the persistent hydrophobic defects into a single large cavity. First, this simulation assumed a planar bilayer, because the extension to curved membranes is not yet theoretically feasible. J. Bentz and A. Mittal (manuscript in preparation) have shown that the model of HA aggregation forming curved domes proposed by Kozlov and Chernomordik (1998) is consistent with the kinetic analysis of fusion data for HA-expressing cells and virions (Bentz, 2000a, Mittal and Bentz, 2001; Mittal et al., 2002b). Thus, the beginning point for the fusogenic aggregate should be a lipid dome tightly ringed by the aggregated HAs. This produces an elastic energy at the peak of the dome due to its curvature. However, the dome rises less than 3 nm above the base of HA, i.e., the target membrane is at least 6 to 8 nm away. One way to minimize the elastic energy of the curved dome would be to percolate the hydrophobic defects to its peak, thereby creating a single cavity. Second, there was no hydrophobic barrier around the inner monolayer required to mimic the other half of the transmembrane domain. With membrane curvature, the defect monolayer would be thinner than the intact monolayer in the first place; hence the defect monolayer would not be able to thin as much as in the planar case. On the other hand, the thicker inner monolayer would be restrained by the hydrophobic perimeter from further commitment to the defect in the outer monolayer. This too would promote the percolation of persistent hydrophobic defects to the peak of the dome because thinning would be relatively inhibited.

The molecular mechanism of HA-mediated fusion is an important and unsolved problem. Many tools have been brought to bear fruitfully on the problem. Simulating the whole fusion site is not feasible at this time. Here, we have mimicked some of the essential elements of one proposed molecular mechanism and found that a rigorous molecular simulation of that simplification has provided a first guess as to how the fusion site needs to evolve to end up at fusion rather than hemifusion. Further simulations can test other

proposed elements of the fusion site, which should lead to the construction of definitive experiments.

D.P.T. is a Scholar of the Alberta Heritage Foundation for Medical Research.

REFERENCES

Armstrong, R. T., A. S. Kushnir, and J. M. White. 2000. The transmembrane domain of influenza hemagglutinin exhibits a stringent length requirement to support the hemifusion to fusion transition. *J. Cell Biol.* 151:425–437.

Bentz, J. 2000a. Minimal aggregate size and minimal fusion unit for the first fusion pore of influenza hemagglutinin mediated membrane fusion. *Biophys. J.* 78:227–245.

Bentz, J. 2000b. Membrane fusion mediated by coiled coils: a hypothesis. *Biophys. J.* 78:886–900.

Bentz, J., and H. Ellens. 1988. Membrane fusion: kinetics and mechansims. *Colloids Surf.* 30:65–112.

Bentz, J., and A. Mittal. 2000. Deployment of membrane fusion protein domains during fusion. *Cell Biol. Int.* 24:819–838.

Berendsen, H. J. C., J. P. M. Postma, W. F. van Gunsteren, and J. Hermans. 1981. Intermolecular Forces. Reidel, Dordrecht, The Netherlands.

Berendsen, H. J. C., J. P. M. Postma, W. F. van Gunsteren, A. DiNola, and J. R. Haak. 1984. Molecular dynamics with coupling to an external bath. *J. Chem. Phys.* 81:3684–3690.

Berendsen, H. J. C., D. van der Spoel, and R. van Drunen. 1995. GROMACS: a message-passing parallel molecular dynamics implementation. *Comp. Phys. Commun.* 95:43–56.

Berger, O., O. Edholm, and F. Jahnig. 1997. Molecular dynamics simulations of a fluid bilayer of dipalmitoylphosphatidylcholine at full hydration, constant pressure, and constant temperature. *Biophys. J.* 72: 2002–2013.

Chernomordik, L. 1996. Non-bilayer lipids and biological fusion intermediates. *Chem. Phys. Lipids.* 81:203–213.

Chernomordik, L. V., V. A. Frolov, E. Leikina, P. Bronk, and J. Zimmerberg. 1998. The pathway of membrane fusion catalyzed by influenza hemagglutinin: restriction of lipids, hemifusion, and lipid fusion pore formation. *J. Cell Biol.* 140:1369–1382.

Eckert, D. M., and P. S. Kim. 2001. Mechanisms of viral membrane fusion and its inhibition. *Annu. Rev. Biochem.* 70:777–810.

Feller, S. E. 2000. Molecular dynamics simulations of lipid bilayers. *Curr. Opin. Colloid Interface Sci.* 5:217–223.

Kim, C., J. C. Macosko, and Y. K. Shin. 1998. The mechanism of low-pH-induced clustering of phospholipid vesicles carrying the HA2 ectodomain of influenza hemagglutinin. *Biochemistry.* 37:137–144.

Kozlov, M. M., and L. V. Chernomordik. 1998. A mechanism of protein-mediated fusion: coupling between refolding of the influenza hemagglutinin and lipid rearrangements. *Biophys. J.* 75:1384–1396.

Kozlovsky, Y., and M. M. Kozlov. 2002. Stalk model of membrane fusion: solution of energy crisis. *Biophys. J.* 82:882–895.

Kraulis, P. J. 1991. MOLSCRIPT: a program to produce both detailed and schematic plots of protein structures. *J. Appl. Cryst.* 24:946–950.

Kuzmin, P. I., J. Zimmerberg, Y. A. Chizmadzhev, and F. S. Cohen. 2001. A quantitative model for membrane fusion based on low-energy intermediates. *Proc. Natl. Acad. Sci. U. S. A.* 98:7235–7240.

Lentz, B. R., and J. K. Lee. 2000. Poly(ethylene glycol) (PEG)-mediated fusion between pure lipid bilayers: a mechanism in common with viral fusion and secretory vesicle release? *Mol. Membr. Biol.* 16:279–296.

Leikina, E., D. L. LeDuc, J. C. Macosko, R. Epand, R. Epand, Y. K. Shin, and L. V. Chernomordik. 2001. The 1–127 HA2 construct of influenza virus hemagglutinin induces cell-cell hemifusion. *Biochemistry.* 40: 8378–8386.

Lindahl, E., and O. Edholm. 2001. Molecular dynamics simulation of NMR relaxation rates and slow dynamics in lipid bilayers. *J. Chem. Phys.* 115:4938–4950.

Markin, V. S., and J. P. Albanesi. 2002. Membrane fusion: stalk model revisited. *Biophys. J.* 82:693–712.

Marrink, S. J., E. Lindahl, O. Edholm, and A. E. Mark. 2001. Simulation of the spontaneous aggregation of phospholipids into bilayers. *J. Am. Chem. Soc.* 123:8638–8639.

Melikyan, G. B., S. Lin, M. Roth, and F. S. Cohen. 1999. Amino acid sequence requirements of the transmembrane and cytoplasmic domains of influenza virus hemagglutinin required for viable membrane fusion. *Mol. Biol. Cell.* 10:1821–1836.

Merritt, E. A., and D. J. Bacon. 1997. Raster3D: photorealistic molecular graphics. *Methods Enzymol.* 277:505–524.

Mittal, A., and J. Bentz. 2001. Comprehensive kinetic analysis of influenza hemagglutinin mediated membrane fusion: role of sialate binding. *Biophys. J.* 81:1521–1535.

Mittal, A., E. Leikina, L. V. Chernomordik, and J. Bentz. 2001. Monitoring single cell fusion kinetics from automated video fluorescence microscopy. *Mol. Biol. Cell.* 12S:74a.

Mittal, A., E. Leikina, J. Bentz, and L. V. Chernomordik. 2002a. Kinetics of RBC fusion with influenza hemagglutinin-expressing cells as a function of technique. *Anal. Biochem*. 303:145–152.

Mittal, A., T. Shangguan, and J. Bentz. 2002b. Measuring pKa of activation and pKi of inactivation for influenza hemagglutinin from kinetics of membrane fusion of virions and of HA expressing cells. *Biophys. J.* In press.

Moore, P. B., C. F. Lopez, and M. L. Klein. 2001. Dynamical properties of a hydrated lipid bilayer from a multinanosecond molecular dynamics simulation. *Biophys. J.* 81:2484–2494.

Nagle, J. F., R. Zhang, S. Tristram-Nagle, W. Sun, H. I. Petrache, and R. M. Suter. 1996. X-ray structure determination of fully hydrated L alpha phase dipalmitoylphosphatidylcholine bilayers. *Biophys. J.* 70: 1419–1431.

Qiao, H., R. Armstrong, G. B. Melikyan, F. G. S. Cohen, and J. M. White. 1999. A specific point mutation at position 1 of the influenza hemagglutinin peptide displays a hemifusion phenotype. *Mol. Biol. Cell* 10: 2759–2769.

Qiao, H., S. Pelletier, L. Hoffman, J. Hacker, R. Armstrong, and J. M. White. 1998. Specific single or double proline substitutions in the "spring-loaded" coiled coil region of the influenza hemagglutinin impair or abolish membrane fusion activity. *J. Cell Biol.* 141:1335–1347.

Siegel, D. P. 1999. The modified stalk mechanism of lamellar/inverted phase transitions and its implications for membrane fusion. *Biophys. J.* 76:291–313.

Skehel, J. J., and D. C. Wiley. 1998. Coiled coils in both intracellular vesicle and viral membrane fusion. *Cell.* 95:871–874.

Tieleman, D. P., H. J. C. Berendsen, and M. S. P. Sansom. 1999. An alamethicin channel in a lipid bilayer: molecular dynamics simulations. *Biophys. J.* 76:1757–1769.

Tieleman, D. P., S. J. Marrink, and H. J. C. Berendsen. 1997. A computer perspective of membranes: molecular dynamics studies of lipid bilayer systems. *Biochim. Biophys. Acta.* 1331:235–270.

van der Spoel, D., A. R. van Buuren, E. Apol, P. J. Meulenhoff, D. P. Tieleman, A. L. T. M. Sijbers, B. Hess, K. A. Feenstra, E. Lindahl, R. van Drunen, and H. J. C. Berendsen. 1999. Gromacs User Manual, Version 2:0. University of Groningen, Groningen.